

---

# Recurrent Neural Filters: Learning Independent Bayesian Filtering Steps for Time Series Prediction

---

Bryan Lim<sup>1,2</sup> Stefan Zohren<sup>1,2</sup> Stephen Roberts<sup>1,2</sup>

## Abstract

Despite the recent popularity of deep generative state space models, few comparisons have been made between network architectures and the inference steps of the Bayesian filtering framework – with most models simultaneously approximating both state transition and update steps with a single recurrent neural network (RNN). In this paper, we introduce the Recurrent Neural Filter (RNF), a novel recurrent variational autoencoder architecture that learns distinct representations for each Bayesian filtering step, captured by a series of encoders and decoders. Testing this on three real-world time series datasets, we demonstrate that decoupling representations not only improves the accuracy of one-step-ahead forecasts while providing realistic uncertainty estimates, but also facilitates multistep prediction through the separation of encoder stages.

## 1. Introduction

Bayesian filtering (Candy, 2009) has been extensively used within the domain of time series prediction, with numerous applications across different fields – including target tracking (Haug, 2012), robotics (Barfoot, 2017), finance (Ghosh et al., 2015), and medicine (Sukkar et al., 2012). Performing inference via a series of prediction and update steps (Sarkka, 2013), Bayes filters recursively update the posterior distribution of predictions – or the belief state (Thrun et al., 2005) – with the arrival of new data. For many filter models – such as the Kalman filter (Kalman, 1960) and non-linear variants like the unscented Kalman filter (Julier & Uhlmann, 1997) – deterministic functions are used at each step to adjust the

sufficient statistics of the belief state, guided by generative models of the data. Each function quantifies the impact of different sources of information on latent state estimates – specifically time evolution and exogenous inputs in the prediction step, and realised observations in the update step. On top of efficient inference and uncertainty estimation, this decomposition of inference steps enables Bayes filters to be deployed in use cases beyond basic one-step-ahead prediction – with simple extensions for multistep prediction (Harvey, 1991) and prediction in the presence of missing observations (Harvey & Pierse, 1984).

With the increasing use of deep neural networks for time series prediction, applications of recurrent variational autoencoder (RVAE) architectures have been investigated for forecasting non-linear state space models (Chung et al., 2015; Krishnan et al., 2015; Krishnan et al., 2017; Karl et al., 2017). Learning dynamics directly from data, they avoid the need for explicit model specification – overcoming a key limitation in standard Bayes filters. However, these RVAEs focus predominantly on encapsulating the generative form of the state space model – implicitly condensing both state transition and update steps into a single representation learnt by the RVAE decoder – and make it impossible to decouple the Bayes filter steps.

Recent works in deep generative modelling have focused on the use of neural networks to learn independent factors of variation in static datasets – through the encouragement of disentangled representations (Narayanaswamy et al., 2017; Kim & Mnih, 2018) or by learning causal mechanisms (Parascandolo et al., 2018; Thomas et al., 2018). While a wide range of training procedures and loss functions have been proposed (Locatello et al., 2018), methods in general use dedicated network components to learn distinct interpretable relationships – ranging from orthogonalising latent representations in variational autoencoders (Higgins et al., 2017) to learning independent modules for different causal pathways (Parascandolo et al., 2018). By understanding the relationships encapsulated by each component, we can subsequently decouple them for use in related tasks – allowing the learnt mechanisms to generalize to novel domains (Parascandolo et al., 2018; Lake et al., 2017) or to provide building blocks for transfer learning (Higgins et al., 2017).

---

<sup>1</sup>Oxford-Man Institute of Quantitative Finance, University of Oxford, Oxford, United Kingdom <sup>2</sup>Department of Engineering Science, University of Oxford, Oxford, United Kingdom. Correspondence to: Bryan Lim <bryan.lim@eng.ox.ac.uk>, Stefan Zohren <zohren@robots.ox.ac.uk>, Stephen Roberts <sjrob@robots.ox.ac.uk>.

In this paper, we introduce the Recurrent Neural Filter (RNF) – a novel variational autoencoder (VAE) architecture which aligns network modules (encoders and decoders) with the inference steps of the Bayes filter – making several contributions over standard VAE approaches. Firstly, we propose a new training procedure to encourage independent representations within each module, by directly training intermediate encoders with a common emission decoder. In doing so, we augment the VAE loss function with additional regularisation terms (see Section 4.2), and directly encourage each encoder to learn functions to update the filter’s belief state given available information. Furthermore, we randomly skip RNN memory updates during training, reducing sensitivity to the sequence of the encoder stages. Next, we highlight performance gains for one-step-ahead predictions through experiments on a variety of real-world time series datasets – reflecting the benefits of improved representation learning by the RNF. Lastly, we investigate multi-step predictions as a potential use case for generalising the decoupled representations of the RNF to other tasks – demonstrating performance improvements from the recursive application of the state transition encoders alone.

## 2. Related Work

**RVAEs for State Space Modelling:** The work of Chung et al. (2015) identifies close parallels between RNNs and latent state space models, both consisting of an internal hidden state that drives output forecasts and observations. Using a RVAE architecture described as a variational RNN (VRNN), they build their recognition network (encoder) with RNNs and produce samples for the stochastic hidden state at each time point. Deep Kalman filters (DKFs) (Krishnan et al., 2015; Krishnan et al., 2017) take this a step further by allowing for exogenous inputs in their network and incorporating an additional KL loss term to penalise state transitions between time steps. Deep Variational Bayes Filters (DVBFs) (Karl et al., 2017) enhance the interpretability of DKFs by modelling state transitions with parametric – e.g. linear – models, which take in stochastic samples from the recognition model as inputs. In general, while the above models capture the generative modelling aspects of the state space framework, their inference procedure blends both state transition and error correction steps, obliging the recognition model to simultaneously learn representations for both. In contrast, the RNF uses separate neural network components to directly model the Bayes filter steps – leading to improvements in representation learning and enhanced predictive performance in time series applications.

**Hybrid Approaches:** In Johnson et al. (2016) the authors take a hybrid approach with the structured variational autoencoder (SVAE), proposing an efficient general inference framework that combines probabilistic graphical mod-

els for the latent state with neural network observation models. This is similar in spirit to the Kernel Kalman Filter (Ralaivola & d’Alche Buc, 2005), allowing for predictions to be made on complex observational datasets – such as raw images – by encoding high dimensional outputs onto a lower dimensional latent representation modelled with a dynamical systems model. Although SVAEs provide a degree of interpretability to temporal dynamics, they also require a parametric model to be defined for the latent states which may be challenging for arbitrary time series datasets. The RNF, in comparison, is able to learn the relationships directly from data, without the need for explicit model specification. The Kalman variational autoencoder (KVAE) (Fraccaro et al., 2017) extends ideas from the SVAE, modelling latent state using a linear Gaussian state space model (LGSSM). To allow for non-linear dynamics, the KVAE uses a recognition model to produce time-varying parameters for the LGSSM, weighting a set of  $K$  constant parameters using weights generated by a neural network. Deep State Space Models (DSSM) (Rangapuram et al., 2018) investigate a similar approach within the context of time series prediction, using a RNN to generate parameters of the LGSSM at each time step. While the LGSSM components do allow for the application of the Kalman filter, we note that updates to the time-varying weights from the RNN once again blend the prediction and update steps – making the separation of Bayes filter steps and generalisation to other tasks non-trivial. On the other hand, the RNF naturally supports simple extensions (e.g. multistep prediction) in a similar fashion to other Bayes filter – due to the close alignment of the RNF architecture with the Bayes filter steps and the use of decoupled representations across encoders and decoders.

**Predictive State Representations:** Predictive state RNNs (PSRNN) (Choromanski et al., 2018; Downey et al., 2017; Venkatraman et al., 2017) use an alternative formulation of the Bayes filter, utilising a state representation that corresponds to the statistics of a distribution for future observations. Predictions are made using a two-stage regression approach modelled by their proposed architectures. Compared to alternative VAE approaches, PSRNNs only produce point estimates for their forecasts – lacking the uncertainty bounds from predictive distributions produced by the RNF.

**Non-Parametric State Space Models:** Gaussian Process state space models (GP-SSMs) (Turner et al., 2010; Nickisch et al., 2018) and variational approximations (Doerr et al., 2018), provide an alternative non-parametric approach to forecasting non-linear state space models – modelling hidden states and observation dynamics using GPs. While they have similar benefits to Bayes filters (i.e. predictive uncertainties, natural multistep prediction etc.), inference at each time step has at least an  $O(T)$  complexity in the number of past observations – either via sparse GP approximations or Kalman filter formulations (Sarkka et al., 2013).

In contrast, the RNF updates its belief state at each time point only with the latest observations and input, making it suitable for real-time prediction on high-frequency datasets.

### 3. Problem Definition

Let  $\mathbf{y}_t = [y_t(1), \dots, y_t(O)]^T$  be a vector of observations, driven by a set of stochastic hidden states  $\mathbf{x}_t = [x_t(1), \dots, x_t(J)]^T$  and exogenous inputs  $\mathbf{u}_t = [u_t(1), \dots, u_t(I)]^T$ . We consider non-linear state space models of the following form:

$$\mathbf{y}_t \sim \Pi(f(\mathbf{x}_t)) \quad (1)$$

$$\mathbf{x}_t \sim N(\mu(\mathbf{x}_{t-1}, \mathbf{u}_t), \Sigma(\mathbf{x}_{t-1}, \mathbf{u}_t)) \quad (2)$$

where  $\Pi$  is an arbitrary distribution parametrised by a non-linear function  $f(\mathbf{x}_t)$ ,  $\mu(\cdot)$  and  $\Sigma(\cdot)$  are mean and covariance functions respectively.

Bayes filters allow for efficient inference through the use of a belief state, i.e. a posterior distribution of hidden states given past observations  $\mathbf{y}_{1:t} = \{\mathbf{y}_1, \dots, \mathbf{y}_t\}$  and inputs  $\mathbf{u}_{1:t} = \{\mathbf{u}_1, \dots, \mathbf{u}_t\}$ . This is achieved through the maintenance of a set sufficient statistics  $\boldsymbol{\theta}_t$  – e.g. means and covariances  $\boldsymbol{\theta}_t \in \{\boldsymbol{\mu}_t, \boldsymbol{\Sigma}_t\}$  – which compactly summarise the historical data:

$$p(\mathbf{x}_t | \mathbf{y}_{1:t}, \mathbf{u}_{1:t}) = \text{bel}(\mathbf{x}_t; \boldsymbol{\theta}_t) \quad (3)$$

$$= N(\mathbf{x}_t; \boldsymbol{\mu}_t, \boldsymbol{\Sigma}_t) \quad (4)$$

where  $\text{bel}(\cdot)$  is a probability distribution function for the belief state.

For filters such as the Kalman filter – and non-linear variants like the unscented Kalman filter (Julier & Uhlmann, 1997) –  $\boldsymbol{\theta}_t$  is recursively updated through a series of prediction and update steps which take the general form below:

#### Prediction (State Transition):

$$\tilde{\boldsymbol{\theta}}_t = \phi_u(\boldsymbol{\theta}_{t-1}, \mathbf{u}_t) \quad (5)$$

#### Update (Error Correction):

$$\boldsymbol{\theta}_t = \phi_y(\tilde{\boldsymbol{\theta}}_t, \mathbf{y}_t) \quad (6)$$

where  $\phi_u(\cdot)$  and  $\phi_y(\cdot)$  are non-linear deterministic functions. Forecasts can then be computed using one-step ahead predictive distributions:

$$p(\mathbf{y}_t | \mathbf{y}_{1:t-1}, \mathbf{u}_{1:t}) = \int p(\mathbf{y}_t | \mathbf{x}_t) \text{bel}(\mathbf{x}_t; \tilde{\boldsymbol{\theta}}_t) d\mathbf{x}_t. \quad (7)$$

## 4. Recurrent Neural Filter

In this section, we describe the Recurrent Neural Filter (RNF) – which models the steps of the Bayes filter algorithm using a VAE approach. A full description of the network can be found in Section 4.1, along with an architecture diagram in Figure 1.

### 4.1. Network Architecture

First, we introduce a latent state  $\mathbf{s}_t$  that maps to sufficient statistics  $\boldsymbol{\theta}_t$ , which are obtained as outputs from our recognition model. As per Equations (5) and (6), inference at runtime is controlled through the recursive update of  $\mathbf{s}_t$ , using a series of Long Short-Term Memory (LSTM) (Hochreiter & Schmidhuber, 1997) encoders with exponential linear unit (ELU) activations (Clevert et al., 2016).

#### 4.1.1. ENCODER

To more directly estimate the impact of exogenous inputs on the belief state of the filter, the prediction step, Equation (5), is divided into two parts with separate LSTM units  $\phi_x(\cdot)$  and  $\phi_u(\cdot)$ . We use  $\mathbf{h}_t$  to represent all required memory components – i.e. both output vector and cell state for the standard LSTM – with  $\mathbf{s}_t$  being the output of the cell. A third LSTM cell  $\phi_y(\cdot)$  is then used for the update step, Equation (6), with the full set of equations below.

#### Prediction:

$$\text{Propagation} \quad [\tilde{\mathbf{s}}'_t, \tilde{\mathbf{h}}'_t] = \phi_x(\mathbf{h}_{t-1}) \quad (8)$$

$$\text{Input Dynamics} \quad [\tilde{\mathbf{s}}_t, \tilde{\mathbf{h}}_t] = \phi_u(\tilde{\mathbf{h}}'_t, \mathbf{u}_t) \quad (9)$$

#### Update:

$$\text{Error Correction} \quad [\mathbf{s}_t, \mathbf{h}_t] = \phi_y(\tilde{\mathbf{h}}_t, \mathbf{y}_t) \quad (10)$$

To approximate the posterior distribution of  $\mathbf{x}_t$  |  $\{\mathbf{y}_{1:t-1}, \mathbf{u}_{1:t}\}$ , we model  $\mathbf{x}_t$  as multivariate Gaussian:

$$\mathbf{x}_t \sim N(m(\tilde{\mathbf{s}}_t), V(\tilde{\mathbf{s}}_t)) \quad (11)$$

$$m(\tilde{\mathbf{s}}_t) = \mathbf{W}_m \tilde{\mathbf{s}}_t + \mathbf{b}_m \quad (12)$$

$$V(\tilde{\mathbf{s}}_t) = \text{diag}(\sigma(\tilde{\mathbf{s}}_t) \odot \sigma(\tilde{\mathbf{s}}_t)) \quad (13)$$

$$\sigma(\tilde{\mathbf{s}}_t) = \text{Softplus}(\mathbf{W}_\sigma \tilde{\mathbf{s}}_t + \mathbf{b}_\sigma) \quad (14)$$

where  $\mathbf{W}_{(\cdot)}$ ,  $\mathbf{b}_{(\cdot)}$  are the weights and biases of each layer, and  $\odot$  is an element-wise (Hadamard) product.

#### 4.1.2. DECODER

Given a hidden state sample  $\mathbf{x}_t$  as observation, we use a multi-layer perceptron to model the emission function  $f(\cdot)$ , i.e.:

$$f(\mathbf{x}_t) = \mathbf{W}_{x_2} \text{ELU}(\mathbf{W}_{x_1} \mathbf{x}_t + \mathbf{b}_{x_1}) + \mathbf{b}_{x_2}. \quad (15)$$

This allows us to handle both continuous and binary observations using the output models below:

$$\mathbf{y}_t^{\text{continuous}} \sim N\left(f(\mathbf{x}_t), \boldsymbol{\Gamma}\right) \quad (16)$$

$$\mathbf{y}_t^{\text{binary}} \sim \text{Bernoulli}\left(\text{Sigmoid}(f(\mathbf{x}_t))\right) \quad (17)$$

where  $\boldsymbol{\Gamma} = \text{diag}(\rho_1^2, \dots, \rho_j^2)$  is a constant covariance matrix for observation noise.

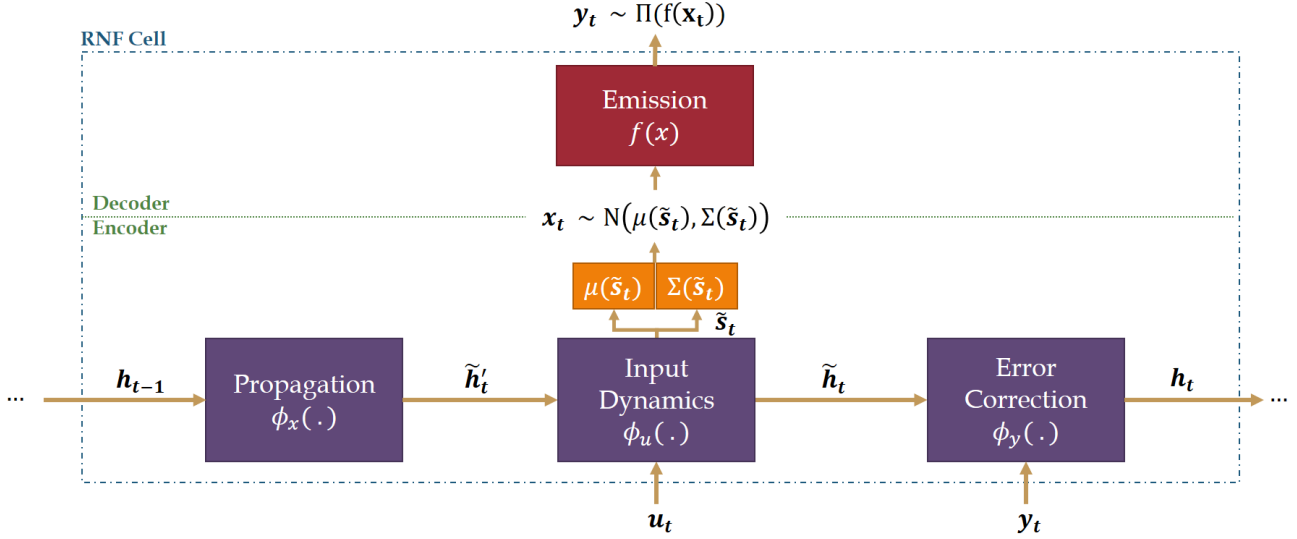


Figure 1. RNF Network Architecture

## 4.2. Training Procedure

Considering the joint observation probabilities for a trajectory of length  $T$ , the evidence lower bound (ELBO) for the variational approximation of Section 4.1 is:

$$ELBO(\omega, \mathbf{y}_{1:T}, \mathbf{u}_{1:T}) = \sum_{t=1}^T \mathbb{E}_{q(\mathbf{x}_t | \tilde{\mathbf{s}}_t)} [\log p(\mathbf{y}_t | \mathbf{x}_t)] - KL(q(\mathbf{x}_1, \dots, \mathbf{x}_T) || p(\mathbf{x}_1, \dots, \mathbf{x}_T)), \quad (18)$$

where  $\omega$  are the weights of the deep neural network,  $q(\mathbf{x}_t | \tilde{\mathbf{s}}_t)$  is the output of our recognition model parameterised by  $\phi_u(\cdot)$ , and  $KL(\cdot)$  is the KL divergence between our recognition network and the prior (see Section 4.2.1).

Using the generative model for  $\mathbf{x}_t$  in Equation (2) to define a general prior, we can adopt the Stochastic Gradient Variational Bayes (SGVB) estimator of Kingma & Welling (2014), expressing our loss function as:

$$\mathcal{L}(\omega, \tilde{\mathbf{s}}_{1:T}) = \sum_{t=1}^T \left\{ \frac{1}{L} \sum_{i=1}^L \log p(\mathbf{y}_t | \mathbf{x}_t^{(i)}(\tilde{\mathbf{s}}_t)) \right\} - KL(q(\mathbf{x}_1, \dots, \mathbf{x}_T) || p(\mathbf{x}_1, \dots, \mathbf{x}_T)), \quad (19)$$

where  $L$  is the number of samples used for calibration,  $\mathbf{x}_k^{(i)}(\tilde{\mathbf{s}}_k)$  is the  $i$ -th sample given the latent state  $\tilde{\mathbf{s}}_k$ .

Considering the emission model for continuous observations in Equation (16), the Gaussian observation log likelihood can be expressed as:

$$\log p(\mathbf{y}_t | \mathbf{x}_t^{(i)}(\tilde{\mathbf{s}}_t)) = -\frac{1}{2} \sum_{j=1}^J \left\{ \log(2\pi\rho_j^2) \right.$$

$$\left. + \left\| \frac{\mathbf{y}_t(j) - f(j, \mathbf{x}_t^{(i)}(\tilde{\mathbf{s}}_t))}{\rho_j} \right\|^2 \right\}, \quad (20)$$

where  $f(j, \mathbf{x}_t^{(i)}(\tilde{\mathbf{s}}_t))$  is the  $j$ -th element of  $f(\mathbf{x}_t^{(i)}(\tilde{\mathbf{s}}_t))$ . To ensure that  $\gamma_j$  remains positive, we implemented this as  $\rho_j = \text{Softplus}(r_j)$ , where  $r_j$  is a variable to be optimised.

### 4.2.1. PRIOR SPECIFICATION AND KL DIVERGENCE

The flexibility of the generative model for  $\mathbf{x}_t$  in Equation (2) allows for a variety of conditional Gaussian priors – potentially with non-linear state transition models. Assuming no domain-specific knowledge regarding latent state dynamics, we consider the two simple priors defined below:

**Linear Gaussian Prior (RNF-LG):** As linear Gaussian state transition models are the foundation of Kalman filtering, they provide a good starting point for state dynamics:

$$\mathbf{x}_t = \mathbf{A}\mathbf{x}_{t-1} + \mathbf{B}\mathbf{u}_t + \mathbf{e}_t \quad (21)$$

Where  $\mathbf{A} \in \mathbb{R}^{J \times J}$  and  $\mathbf{B} \in \mathbb{R}^{J \times I}$  are constant matrices,  $\mathbf{e}_t \sim N(\mathbf{0}, \mathbf{\Omega})$  is a noise term with constant covariance  $\mathbf{\Omega} = \text{diag}(\omega(1)^2, \dots, \omega(J)^2)$ . This enables the derivation of the analytical KL divergence term below, with a full details in Appendix A:

$$KL(q(\mathbf{x}_1, \dots, \mathbf{x}_T) || p(\mathbf{x}_1, \dots, \mathbf{x}_T)) = \frac{1}{2} \sum_{t=1}^T \left( \frac{\det(\mathbf{\Sigma}_p(t))}{\det(\mathbf{\Sigma}_t)} - J + \text{tr}(\mathbf{\Sigma}_p(t)^{-1} \mathbf{\Sigma}_t) + (\boldsymbol{\mu}_p(t) - \boldsymbol{\mu}_t)^T \mathbf{\Sigma}_p(t)^{-1} (\boldsymbol{\mu}_p(t) - \boldsymbol{\mu}_t) \right) \quad (22)$$

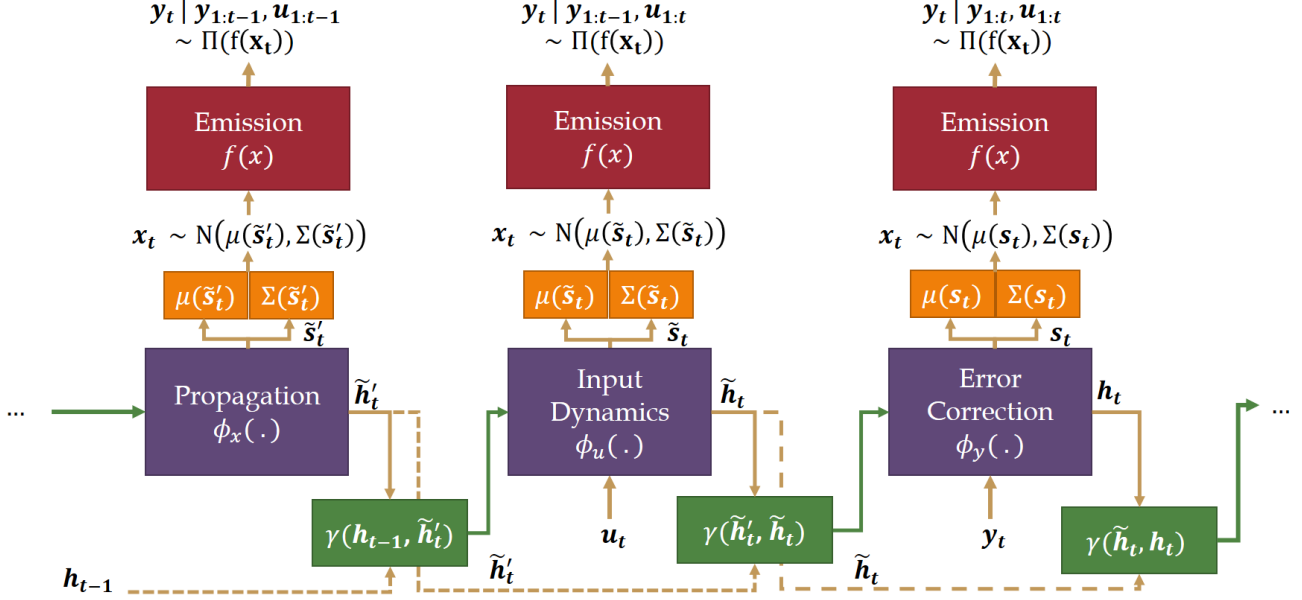


Figure 2. Training Configuration of the RNF

Where  $\mu_t = m(\tilde{s}_t)$ ,  $\Sigma_t = V(\tilde{s}_t)$ ,  $\mu_p(t) = A\mu_{t-1} + Bu_t$  and  $\Sigma_p(t) = A\Sigma_{t-1}A^T + \Omega$ .

**Flat Prior (RNF-NP):** Much recent work has demonstrated the sensitivity of VAE performance to the choice of prior distribution, with suboptimal priors either having an “over-regularising” effect on the loss function during training (Takahashi et al., 2018; Tomczak & Welling, 2018; Bowman et al., 2015), or leading to posterior collapse (van den Oord et al., 2017). As methods to mitigate these effects are still areas of active research (see references in He et al. (2019) and Tomczak & Welling (2018)), we also train the RNF without the KL regularisation terms – which can be interpreted as placing a flat prior over the latent state and removing constants from the VAE loss function. This allows us to quantify improvements which are attributable to the architecture itself, setting a baseline on performance upon which more sophisticated prior models can improve.

#### 4.2.2. ENCOURAGING DECOUPLED REPRESENTATIONS

To learn decoupled representations for the Bayesian filtering steps, the network is slightly rearranged at training time, reflecting the belief state at each stage as seen in Figure 2. The same emission function  $f(\cdot)$  is applied to each encoder, transforming  $x_t$  samples as each encoder updates the hidden state statistics with available information. While standard one-step-ahead prediction uses only the outputs of the input dynamics encoder alone, we train all encoders jointly trained the combined loss function below. The inclusion of additional stages can also be interpreted as to regularisation

terms for the standard VAE loss – weighted by constants  $\alpha_x$  and  $\alpha_y$  to controls the relative importance of the intermediate encoder representations. In our experiments, we place equal importance on all encoders, i.e.  $\alpha_x = \alpha_y = 1$ , to facilitate the subsequent separation of stages for multistep prediction.

$$\begin{aligned}
 \mathcal{L}_{\text{combined}}(\omega, \mathbf{y}_{1:T}, \mathbf{u}_{1:T}) &= \underbrace{\mathcal{L}(\omega, \tilde{\mathbf{s}}_{1:T})}_{\text{Input Dynamics}} + \underbrace{\alpha_x \mathcal{L}(\omega, \tilde{\mathbf{s}}'_{1:T})}_{\text{Propagation}} + \underbrace{\alpha_y \mathcal{L}(\omega, \mathbf{s}_{1:T})}_{\text{Error Correction}} \quad (23) \\
 &= - \sum_{t=1}^T \left\{ \underbrace{\frac{1}{L} \sum_{i=1}^L \log p(\mathbf{y}_t | \mathbf{x}_t^{(i)}(\tilde{\mathbf{s}}_t))}_{\text{Likelihood Loss}} \right. \\
 &\quad \left. - \underbrace{KL(q(\mathbf{x}_1, \dots, \mathbf{x}_T) || p(\mathbf{x}_1, \dots, \mathbf{x}_T))}_{\text{KL Regularisation}} \right\} \\
 &\quad + \underbrace{\alpha_x \mathcal{L}(\omega, \tilde{\mathbf{s}}'_{1:T}) + \alpha_y \mathcal{L}(\omega, \mathbf{s}_{1:T})}_{\text{Additional Regularisation Terms}}. \quad (24)
 \end{aligned}$$

The error correction component  $\phi_y(\cdot)$  can also be interpreted as an auto-encoding step for the latest observation, recovering distributions of  $\mathbf{y}_t$  based on filtered distributions of  $\mathbf{x}_t | \mathbf{y}_{1:t}, \mathbf{u}_{1:t}$ . This hence obliges the network to learn representations for  $\mathbf{x}_t$  and  $\mathbf{s}_t$  that are able to reconstruct the current observation when it is available.

Next, to encourage the independence of stages for other predictive tasks, we also randomly skip across memory updates at training time using skip function  $\gamma(\cdot)$ . For instance, the

skip function for the propagation encoder is:

$$\gamma(\mathbf{h}_{t-1}, \tilde{\mathbf{h}}'_t) = \mathcal{U} \times \mathbf{h}_{t-1} + (1 - \mathcal{U}) \times \tilde{\mathbf{h}}'_t \quad (25)$$

where  $\mathcal{U} \sim \text{Bernoulli}(0.5)$  for each encoder and timestep.

As such, the skip updates introduce artificial missingness into the dataset – obliging encoders to learn functions for updating latent state statistics which are independent of which the previous encoder stage. This independence then facilitates the decoupling of stages for generalisation to related tasks, as seen in other Bayes filters.

### 4.3. Handling Missing Data and Multistep Prediction

One-step-ahead predictions can be computed by sampling from the RNF decoder at each time steps – taking the form below for continuous observations:

$$\mathbb{E}[\mathbf{y}_{t+1} | \mathbf{y}_{1:t}, \mathbf{u}_{1:t+1}] \approx \frac{1}{L} \sum_{i=1}^L f(\mathbf{x}_{t+1}^{(i)}(\tilde{\mathbf{s}}_{t+1})). \quad (26)$$

In addition, the update of  $\tilde{\mathbf{s}}_k$  can also be expressed explicitly in terms of the inputs and observations available at time  $k$ . Using Equations (8) - (10) one gets

$$\left[ \tilde{\mathbf{s}}_{t+1}, \tilde{\mathbf{h}}_{t+1} \right] = \phi_u(\Phi_x(\Phi_y(\tilde{\mathbf{h}}_t, \mathbf{y}_t)), \mathbf{u}_{t+1}), \quad (27)$$

where  $\Phi_y(\cdot), \Phi_x(\cdot)$  are the equivalent of  $\phi_y(\cdot), \phi_u(\cdot)$ , but return only the full memory state (i.e. the  $\mathbf{h}_t$  component).

When data is unavailable, we can separate the encoders, updating  $\mathbf{s}_t$  only when information exists. For instance, to compute multistep forecasts where inputs are not known beforehand, we can recursively apply the state propagation encoder alone – using the form below for a  $\tau$ -step-ahead forecast for continuous observations:

$$\mathbb{E}[\mathbf{y}_{t+\tau} | \mathbf{y}_{1:t}, \mathbf{u}_{1:t}] \approx \frac{1}{L} \sum_{i=1}^L f(\mathbf{x}_{t+\tau}^{(i)}(\tilde{\mathbf{s}}'_{t+\tau}))$$

$$\left[ \tilde{\mathbf{s}}'_{t+\tau}, \tilde{\mathbf{h}}'_{t+\tau} \right] = \phi_x(\Phi_x^{\tau-1}(\mathbf{h}_t))$$

where  $\Phi_x^\tau(\cdot) = \Phi_x(\Phi_x^{\tau-1}(\cdot))$  refers the repeated application of the  $\Phi_x(\cdot)$  function. In cases when inputs are know, we can use a combination of both the propagation and input dynamics encoder as below:

$$\mathbb{E}[\mathbf{y}_{t+\tau} | \mathbf{y}_{1:t}, \mathbf{u}_{1:t+\tau}] \approx \frac{1}{L} \sum_{i=1}^L f(\mathbf{x}_{t+\tau}^{(i)}(\tilde{\mathbf{s}}_{t+\tau}))$$

$$\left[ \tilde{\mathbf{s}}_{t+\tau}, \tilde{\mathbf{h}}_{t+\tau} \right] = \phi_u\left(\phi_x(\Phi_{x,u}^{\tau-1}(\mathbf{h}_t, \mathbf{u}_{t+1:t+\tau-1})), \mathbf{u}_{t+\tau}\right)$$

where  $\Phi_{x,u}^{\tau-1}(\cdot)$  refers to the recursive application of both encoders, i.e.  $\Phi_{x,u}^1(\mathbf{h}_t, \mathbf{u}_{t+1}) = \Phi_u(\Phi_x(\mathbf{h}_t), \mathbf{u}_{t+1})$ .

## 5. Performance Evaluation

We conduct a series of tests on 3 real-world time series datasets to evaluate performance, adopting use cases in which real-time prediction with RNNs are most beneficial – i.e. when the underlying dynamics is highly non-linear, and trajectories are long. A brief description of the data can be found below, with full details documented in Appendix B.

### 5.1. Time Series Datasets

**Electricity:** The UCI Individual Household Electric Power Consumption Dataset (Dheeru & Karra Taniskidou, 2017) is a time series of 7 different power consumption metrics measured at 1-min intervals for a single household between December 2006 and November 2010 – coming to a total of 2,075,259 time steps over 4 years. In our experiments, we treated active power as the main observation of interest, taking the remainder to be exogenous inputs into the RNNs.

**Intraday Volatility:** We compute 30-min realised variances (Andersen et al., 2003) for a universe of 30 different stock indices – derived using 1-min index returns subsampled from Thomson Reuters Tick History Level 1 (TRTH L1) quote data. On the whole, the entire dataset contains 1,706,709 measurements across all indices, with each trajectory spanning 17 years on average. Given the strong evidence for the intraday periodicity of returns volatility (Andersen & Bollerslev, 1997), we also include the time-of-day as an additional exogenous input.

**High-Frequency Stock Quotes:** This dataset consists of extracted features from TRTH L1 stock quote data for Barclays (BARC.L) – specifically forecasting microprice returns (Todd et al., 2014) using volume imbalance as an input predictor (see Appendix B) – comprising a total of 29,321,946 time steps between 03 January 2017 to 29 December 2017. From (Cartea et al., 2018), volume imbalance in the limit order book has been shown to be a good predictor of the direction (sign) of the next liquidity taking order, and the price changes immediately after the arrival of a liquidity taking order.

### 5.2. Conduct of Experiment

**Metrics:** To determine the accuracy of forecasts, we evaluate the mean-squared-error (MSE) for single-step and multistep predictions – normalising each using the MSE of the one-step-ahead simple LSTM forecast. As observations are 1D continuous variables for all our datasets, we evaluate uncertainty estimates using the prediction interval coverage probability (PICP) of a 90% prediction interval, defined as:

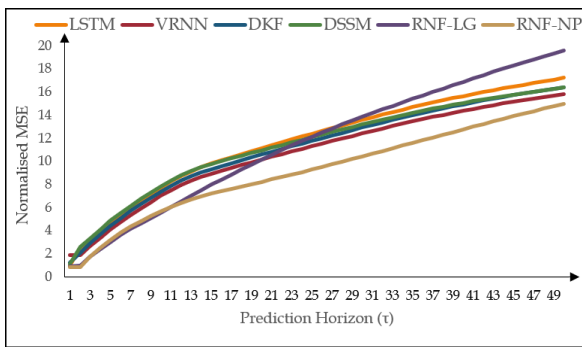
$$\text{PICP} = \frac{1}{T} \sum_{t=1}^T c_t \quad (28)$$

	Electricity	Volatility	Quote
<b>LSTM</b>	1.000	1.000	1.000
<b>VRNN</b>	1.902	5.438	1.042
<b>DKF</b>	1.252	0.980	1.049
<b>DSSM</b>	1.131	7.578	1.048
<b>RNF-LG</b>	0.918	0.997	1.049
<b>RNF-NP</b>	<b>0.856</b>	<b>0.957</b>	<b>0.979</b>

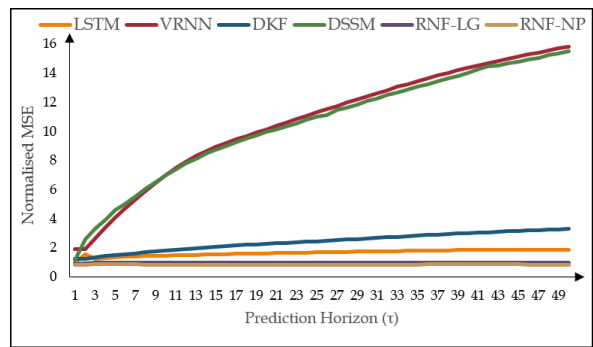
Table 1. Normalised MSEs for One-Step-Ahead Predictions

	Electricity	Volatility	Quote
<b>VRNN</b>	0.986	1.000	0.976
<b>DKF</b>	1.000	1.000	0.995
<b>DSSM</b>	0.964	0.999	0.991
<b>RNF-LG</b>	0.960	1.000	1.000
<b>RNF-NP</b>	0.927	1.000	1.000

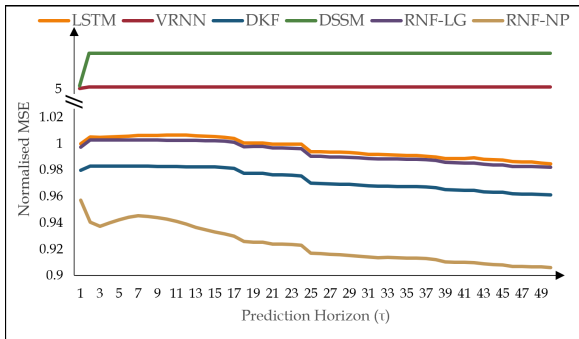
Table 2. Coverage Probability of One-Step-Ahead 90% Prediction Interval



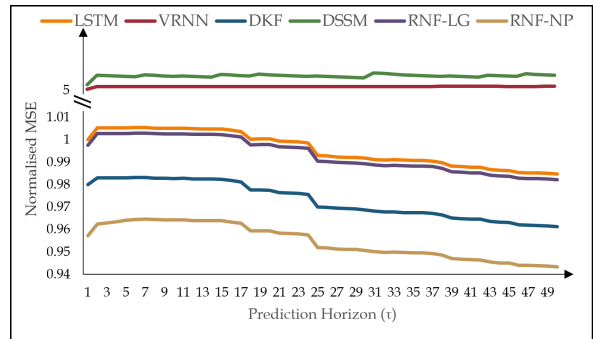
(a) Electricity (Imputed Inputs)



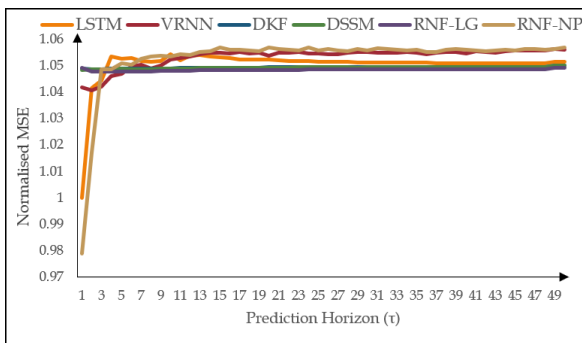
(b) Electricity (Known Inputs)



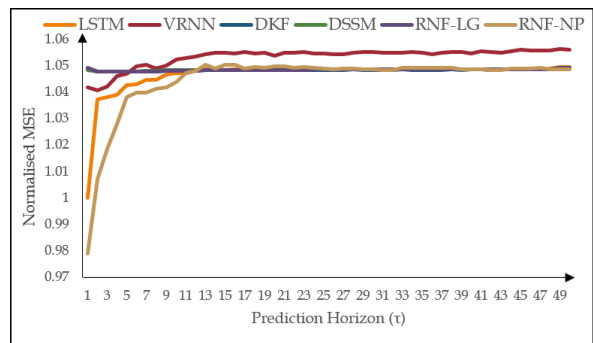
(c) Volatility (Imputed Inputs)



(d) Volatility (Known Inputs)



(e) Quote (Imputed Inputs)



(f) Quote (Known Inputs)

Figure 3. Normalised MSEs for Multistep Predictions

$$c_t = \begin{cases} 1, & \text{if } \psi(0.05, t) < y_t < \psi(0.95, t) \\ 0, & \text{otherwise} \end{cases} \quad (29)$$

where  $\psi(0.05, t)$  is the 5<sup>th</sup> percentile of samples from  $N(f(\mathbf{x}_t), \Gamma)$ . For prediction interval tests, we omitted the pure LSTM benchmark – which is purely deterministic – from our evaluation.

**Benchmarks:** We compare the RNF against a range of RNN and RVAE benchmarks – including the standard LSTM, Variational RNN (VRNN) (Chung et al., 2015), Deep Kalman Filter (DKF) (Krishnan et al., 2015) and Deep State Space Model (DSSM) (Rangapuram et al., 2018).

For multistep prediction, we consider two potential use cases for exogenous inputs: (i) when future inputs are unknown beforehand and imputed using their last observed values, and (ii) when inputs are known in advance and used as given. When models require observations of  $\mathbf{y}_t$  as inputs, we recursively feed outputs from the network as inputs at the next time step. These tweaks allow the benchmarks to be used for multistep prediction without modifying network architectures. For the RNF, we consider the application of the propagation encoder alone for the former case, and a combination of the propagation and input dynamics encoder for the latter – as detailed in Section 4.3.

**Training Details:** During network calibration, trajectories were partitioned into segments of 50 time steps each, and trained up to a maximum of 100 epochs. Hyperparameter optimisation for the Electricity and Volatility datasets was performed using 50 iterations of random search, while random search on the Quote dataset was limited to 20 iterations due to the size of the dataset. For sample sizes, we use  $L = 1$  during training,  $L = 30$  for our validation error and  $L = 100$  for our test MSEs. Full details on optimal hyperparameter configurations and search ranges can be found in Appendix C.

To ensure consistency across all models used, we constrain both the memory state of the LSTM and the latent variable modelled to have the same dimensionality – i.e.  $J = \dim(\mathbf{s}_t) = \dim(\mathbf{x}_t)$  for the RNF. The exception is the DSSM, as the full covariance matrix of the Kalman filter would result in a prohibitive  $J^2$  memory requirement if left unchecked. As such, we use the constraint for both the RNN and the Kalman filter to have the same memory capacity for the DSSM – i.e.  $J = \dim(\mathbf{s}_t) = \dim(\mathbf{x}_t) + \dim(\mathbf{x}_t)^2$ .

### 5.3. Results and Discussion

The benefits of the RNF can be seen from the improvements in both one-step and multi-step normalised MSEs. From the results of Table 1, the RNF-NP has the best performance across all datasets, with average improvements of 8% over the LSTM benchmark, 19% over the DKF, and 2 times and

2.4 times respectively for the VRNN and DSSM. The PICPs in Table 2 also show that improvements are not made at the expense of uncertainty estimates, with prediction intervals spanning more than 90% of the observed outputs for all probabilistic models as expected.

The quality of the representations learnt at each stage can also be seen from the improvements in multi-step prediction accuracy in Figures 3 – with the RNF-NP models demonstrating the best performance in most cases considered. For the Electricity and Volatility Datasets, the RNF-NP demonstrates clear improvements over the other benchmarks for predictive horizons up to  $\tau = 50$ . For the Quote dataset, the RNF-NP demonstrates clear performance gains over all benchmarks over shorter term horizons ( $\tau < 3$  for imputed inputs and  $\tau < 10$  for known inputs), converging to similar error levels as or slightly underperforming (by less than 1%) other benchmarks. In general, RNF multistep performance improvements with imputed inputs show the advantages of applying the propagation stage in isolation, and the benefits of using both the propagation and inputs dynamics encoders when inputs are known in advance.

Comparing the RNF-LG and RNF-NP, we can see the challenges of prior selection for VAEs, with the use of a linear Gaussian prior leading to poorer performance. This echoes findings in previous works which note the potential over-powering effect of the regularisation term, with solutions being an area of active research (see Section 4.2.1 for more details). However, treating the RNF-NP as a baseline for performance, we can see that the framework of the RNF does lead to improvements over competing methods – noting the potential for additional gains with the development of more sophisticated priors.

## 6. Conclusions

In this paper, we introduce a novel recurrent variational autoencoder (RVAE) architecture, which we call the Recurrent Neural Filter (RNF), to learn decoupled representations for the Bayesian filtering steps – consisting of separate encoders for state propagation, input and error correction dynamics, as well as a common decoder to model emission. This is done via an augmented training procedure – with each encoder trained directly with a common emission decoder, while introducing random skips to LSTM memory updates. Based on experiments with three real-world time series datasets, the direct benefits of the architecture can be seen from the improvements in one-step-ahead predictive performance, while maintaining comparable uncertainty estimates to benchmarks. Due to its modular structure and close alignment with Bayes filter steps, we also show the potential to generalise the RNF to similar predictive tasks – as seen from improvements in multistep prediction using extracted state transition encoders.



## 7. Acknowledgments

This work is supported by the Oxford-Man Institute of Quantitative Finance.

## References

- Andersen, T., Bollerslev, T., Diebold, F., and Labys, P. Modeling and forecasting realized volatility. *Econometrica*, 71(2):579–625, 2003.
- Andersen, T. G. and Bollerslev, T. Intraday periodicity and volatility persistence in financial markets. *Journal of Empirical Finance*, 4(2):115 – 158, 1997. ISSN 0927-5398.
- Barfoot, T. D. *State Estimation for Robotics*. Cambridge University Press, New York, NY, USA, 2017.
- Bowman, S. R., Vilnis, L., Vinyals, O., Dai, A. M., Józefowicz, R., and Bengio, S. Generating sentences from a continuous space. *CoRR*, abs/1511.06349, 2015. URL <http://arxiv.org/abs/1511.06349>.
- Candy, J. V. *Bayesian Signal Processing: Classical, Modern and Particle Filtering Methods*. Wiley-Interscience, New York, NY, USA, 2009.
- Cartea, A., Donnelly, R., and Jaimungal, S. Enhancing trading strategies with order book signals. *Applied Mathematical Finance*, 25(1):1–35, 2018.
- Choromanski, K., Downey, C., and Boots, B. Initialization matters: Orthogonal predictive state recurrent neural networks. In *International Conference on Learning Representations (ICLR 2018)*, 2018.
- Chung, J., Kastner, K., Dinh, L., Goel, K., Courville, A. C., and Bengio, Y. A recurrent latent variable model for sequential data. In *Advances in Neural Information Processing Systems 28 (NIPS 2016)*. 2015.
- Clevert, D.-A., Unterthiner, T., and Hochreiter, S. Fast and accurate deep network learning by exponential linear units (ELUs). In *International Conference on Learning Representations (ICLR 2016)*, 2016.
- Dheeru, D. and Karra Taniskidou, E. UCI machine learning repository – individual household electric power consumption data set, 2017. URL <https://archive.ics.uci.edu/ml/datasets>.
- Doerr, A., Daniel, C., Schiegg, M., Duy, N.-T., Schaal, S., Toussaint, M., and Sebastian, T. Probabilistic recurrent state-space models. In *Proceedings of the 35th International Conference on Machine Learning (ICML 2018)*, 2018.
- Downey, C., Hefny, A., Boots, B., Gordon, G. J., and Li, B. Predictive state recurrent neural networks. In *Advances in Neural Information Processing Systems 30 (NIPS 2017)*. 2017.
- Fraccaro, M., Kamronn, S., Paquet, U., and Winther, O. A disentangled recognition and nonlinear dynamics model for unsupervised learning. In *Advances in Neural Information Processing Systems 30 (NIPS 2017)*. 2017.
- Ghosh, H., Gurung, B., and Prajneshu. Kalman filter-based modelling and forecasting of stochastic volatility with threshold. *Journal of Applied Statistics*, 42(3):492–507, 2015.
- Harvey, A. *Forecasting, Structural Time Series Models and the Kalman Filter*. Cambridge University Press, 1991.
- Harvey, A. C. and Pierse, R. G. Estimating missing observations in economic time series. *Journal of the American Statistical Association*, 79(385):125–131, 1984.
- Haug, A. J. *Bayesian estimation and tracking: a practical guide*. John Wiley & Sons, Hoboken, NJ, 2012.
- He, J., Spokoyny, D., Neubig, G., and Berg-Kirkpatrick, T. Lagging inference networks and posterior collapse in variational autoencoders. In *International Conference on Learning Representations (ICLR)*, 2019.
- Higgins, I., Matthey, L., Pal, A., Burgess, C., Glorot, X., Botvinick, M., Mohamed, S., and Lerchner, A. beta-VAE: Learning basic visual concepts with a constrained variational framework. In *International Conference on Learning Representations (ICLR 2017)*, 2017.
- Hochreiter, S. and Schmidhuber, J. Long short-term memory. *Neural Computation*, 9(8):1735–1780, November 1997. ISSN 0899-7667.
- Johnson, M., Duvenaud, D. K., Wiltchko, A., Adams, R. P., and Datta, S. R. Composing graphical models with neural networks for structured representations and fast inference. In *Advances in Neural Information Processing Systems 29 (NIPS 2016)*. 2016.
- Julier, S. J. and Uhlmann, J. K. New extension of the Kalman filter to nonlinear systems. volume 3068, 1997.
- Kalman, R. E. A new approach to linear filtering and prediction problems. *Transactions of the ASME—Journal of Basic Engineering*, 82(Series D):35–45, 1960.
- Karl, M., Soelch, M., Bayer, J., and van der Smagt, P. Deep variational Bayes filters: unsupervised learning of state space models from raw data. In *International Conference on Learning Representations (ICLR 2017)*, 2017.

- Kim, H. and Mnih, A. Disentangling by factorising. In *Proceedings of the 35th International Conference on Machine Learning (ICML 2018)*, 2018.
- Kingma, D. P. and Welling, M. Auto-encoding variational Bayes. In *International Conference on Learning Representations (ICLR 2014)*, 2014.
- Krishnan, R. G., Shalit, U., and Sontag, D. Deep Kalman Filters. *ArXiv e-prints*, 2015. URL <http://arxiv.org/abs/1511.05121>.
- Krishnan, R. G., Shalit, U., and Sontag, D. Structured inference networks for nonlinear state space models. In *Proceedings of the Thirty-First AAAI Conference on Artificial Intelligence (AAAI 2017)*, 2017.
- Lake, B. M., Ullman, T. D., Tenenbaum, J. B., and Gershman, S. J. Building machines that learn and think like people. *Behavioral and Brain Sciences*, 40:e253, 2017. doi: 10.1017/S0140525X16001837.
- Locatello, F., Bauer, S., Lucic, M., Gelly, S., Schölkopf, B., and Bachem, O. Challenging common assumptions in the unsupervised learning of disentangled representations. *CoRR*, abs/1811.12359, 2018. URL <http://arxiv.org/abs/1811.12359>.
- Narayanaswamy, S., Paige, T. B., van de Meent, J.-W., Desmaison, A., Goodman, N., Kohli, P., Wood, F., and Torr, P. Learning disentangled representations with semi-supervised deep generative models. In *Advances in Neural Information Processing Systems 30 (NIPS 2017)*, pp. 5925–5935. 2017.
- Nickisch, H., Solin, A., and Grigorevskiy, A. State space Gaussian processes with non-Gaussian likelihood. In *Proceedings of the 35th International Conference on Machine Learning (ICML 2018)*, pp. 3789–3798, 2018.
- Parascandolo, G., Kilbertus, N., Rojas-Carulla, M., and Schölkopf, B. Learning independent causal mechanisms. In *Proceedings of the 35th International Conference on Machine Learning (ICML 2018)*, 2018.
- Ralaivola, L. and d’Alche Buc, F. Time series filtering, smoothing and learning using the kernel Kalman filter. In *Proceedings. 2005 IEEE International Joint Conference on Neural Networks*, volume 3, pp. 1449–1454, July 2005.
- Rangapuram, S. S., Seeger, M. W., Gasthaus, J., Stella, L., Wang, Y., and Januschowski, T. Deep state space models for time series forecasting. In Bengio, S., Wallach, H., Larochelle, H., Grauman, K., Cesa-Bianchi, N., and Garnett, R. (eds.), *Advances in Neural Information Processing Systems 31 (NeurIPS 2018)*. 2018.
- Sarkka, S. *Bayesian Filtering and Smoothing*. Cambridge University Press, New York, NY, USA, 2013.
- Sarkka, S., Solin, A., and Hartikainen, J. Spatiotemporal learning via infinite-dimensional Bayesian filtering and smoothing: A look at Gaussian process regression through Kalman filtering. *IEEE Signal Processing Magazine*, 30(4):51–61, July 2013.
- Sukkar, R., Katz, E., Zhang, Y., Raunig, D., and Wyman, B. T. Disease progression modeling using hidden Markov models. In *2012 Annual International Conference of the IEEE Engineering in Medicine and Biology Society*, pp. 2845–2848, Aug 2012.
- Takahashi, H., Iwata, T., Yamanaka, Y., Yamada, M., and Yagi, S. Variational autoencoder with implicit optimal priors. *CoRR*, abs/1809.05284, 2018. URL <https://arxiv.org/abs/1809.05284>.
- Thomas, V., Bengio, E., Fedus, W., Pondard, J., Beaudoin, P., Larochelle, H., Pineau, J., Precup, D., and Bengio, Y. Disentangling the independently controllable factors of variation by interacting with the world. In *NIPS 2017 Workshop on Learning Disentangled Representations*, 2018.
- Thrun, S., Burgard, W., and Fox, D. *Probabilistic Robotics (Intelligent Robotics and Autonomous Agents)*. The MIT Press, 2005.
- Todd, A., Hayes, R., Beling, P., and Scherer, W. Micro-price trading in an order-driven market. In *2014 IEEE Conference on Computational Intelligence for Financial Engineering Economics (CIFER)*, pp. 294–297, March 2014.
- Tomczak and Welling. VAE with a VampPrior. In *Proceedings of the 21st International Conference on Artificial Intelligence and Statistics (AISTATS)*, 2018.
- Turner, R., Deisenroth, M., and Rasmussen, C. State-space inference and learning with Gaussian processes. In *Proceedings of the Thirteenth International Conference on Artificial Intelligence and Statistics (AISTATS 2010)*, pp. 868–875, 2010.
- van den Oord, A., Vinyals, O., and Kavukcuoglu, K. Neural discrete representation learning. In *Advances in Neural Information Processing Systems 30 (NIPS)*, pp. 6306–6315. 2017.
- Venkatraman, A., Rhinehart, N., Sun, W., Pinto, L., Hebert, M., Boots, B., Kitani, K., and Bagnell, J. Predictive-state decoders: Encoding the future into recurrent networks. In *Advances in Neural Information Processing Systems 30 (NIPS 2017)*. 2017.

---

## Appendix for Recurrent Neural Filters

---

### A. Derivation of KL Term for RNF-LG

Per Equation (11), we frame  $p(\mathbf{x}_t | \mathbf{y}_{1:t}, \mathbf{u}_{1:t})$  as a multivariate normal distribution with a time varying mean  $\boldsymbol{\mu}_t$  and covariance  $\boldsymbol{\Sigma}_t$ , i.e.  $p(\mathbf{x}_t | \mathbf{y}_{1:t}, \mathbf{u}_{1:t}) \sim N(\boldsymbol{\mu}_t, \boldsymbol{\Sigma}_t)$

From the generative model of Equation (2),  $\log p(\mathbf{x}_1, \dots, \mathbf{x}_T)$  can be factorised as:

$$\begin{aligned} & \log p(\mathbf{x}_1, \dots, \mathbf{x}_T) \\ &= \log p(\mathbf{x}_1) + \sum_{t=2}^T \log p(\mathbf{x}_t | \mathbf{x}_{t-1}, \mathbf{u}_{1:t}, \mathbf{y}_{1:t-1}) \end{aligned} \quad (30)$$

Using the linear Gaussian dynamics of Equation (21), the conditional probabilities can be expressed as:

$$\begin{aligned} & p(\mathbf{x}_t | \mathbf{x}_{t-1}, \mathbf{u}_{1:t}, \mathbf{y}_{1:t-1}) \\ & \sim N(\mathbf{A}\boldsymbol{\mu}_{t-1} + \mathbf{B}\mathbf{u}_t, \mathbf{A}\boldsymbol{\Sigma}_{t-1}\mathbf{A}^T + \boldsymbol{\Omega}) \end{aligned} \quad (31)$$

$$= N(\boldsymbol{\mu}_p(t), \boldsymbol{\Sigma}_p(t)) \quad (32)$$

Conditioning on  $\tilde{\mathbf{s}}_t$ , the recognition model of the RNF allows for the following factorisation:

$$\log q(\mathbf{x}_1, \dots, \mathbf{x}_T) = \sum_{t=1}^T \log q(\mathbf{x}_t | \tilde{\mathbf{s}}_t) \quad (33)$$

$$q(\mathbf{x}_t | \tilde{\mathbf{s}}_t) \sim N(m(\tilde{\mathbf{s}}_t), V(\tilde{\mathbf{s}}_t)) \quad (34)$$

Hence, taking  $\boldsymbol{\mu}_t = m(\tilde{\mathbf{s}}_t)$  and  $\boldsymbol{\Sigma}_t = V(\tilde{\mathbf{s}}_t)$ , the KL divergence can be expressed analytically between conditional Gaussians at each time step, as shown below:

$$\begin{aligned} & KL(q(\mathbf{x}_1, \dots, \mathbf{x}_T) || p(\mathbf{x}_1, \dots, \mathbf{x}_T)) \\ &= \mathbb{E}_{q(\mathbf{x}_1, \dots, \mathbf{x}_T)} \left[ \log \frac{p(\mathbf{x}_1)}{q(\mathbf{x}_1 | \tilde{\mathbf{s}}_1)} \right. \\ & \quad \left. + \sum_{t=2}^T \log \frac{p(\mathbf{x}_t | \mathbf{x}_{t-1}, \mathbf{u}_{1:t}, \mathbf{y}_{1:t-1})}{q(\mathbf{x}_t | \tilde{\mathbf{s}}_t)} \right] \quad (35) \\ &= \frac{1}{2} \sum_{t=1}^T \left( \frac{\det(\boldsymbol{\Sigma}_p(t))}{\det(\boldsymbol{\Sigma}_t)} - J + \text{tr}(\boldsymbol{\Sigma}_p(t)^{-1} \boldsymbol{\Sigma}_t) \right. \\ & \quad \left. + (\boldsymbol{\mu}_p(t) - \boldsymbol{\mu}_t)^T \boldsymbol{\Sigma}_p(t)^{-1} (\boldsymbol{\mu}_p(t) - \boldsymbol{\mu}_t) \right). \end{aligned} \quad (36)$$

### B. Description of Datasets

For the experiments in Section 5, we focus on the use of 3 real-world time series datasets – each containing over a million time steps per dataset – allowing us to evaluate the performance of our proposed method on complex, nonlinear datasets.

#### B.1. Electricity

**Overview** The UCI Individual Household Electric Power Consumption Dataset (Dheeru & Karra Taniskidou, 2017) is a time series of 7 different power consumption metrics measured at 1-min intervals for a single household between December 2006 and November 2010 – coming to a total of 2,075,259 time steps over 4 years. In our experiments, we treated active power as the main observation of interest, taking the remainder to be exogenous inputs into the RNNs.

**Data Processing** The full trajectory was segmented into 3 portions, with the earliest 60% of measurements for training, the next 20% as a validation set, and the final 20% as an independent test set – with results reported in Section 5. All data sets were normalised to have zero mean and unit standard deviations, with normalising constants computed using the training set alone.

**Summary Statistics** A list of summary statistics can be seen in Table 3.

	Mean	S.D.	Min	Max
<b>Active Power*</b>	1.11	1.12	0.08	11.12
<b>Reactive Power</b>	0.12	0.11	0.00	1.39
<b>Intensity</b>	4.73	4.70	0.20	48.40
<b>Voltage</b>	240.32	3.33	223.49	252.72
<b>Sub Metering 1</b>	1.17	6.31	0.00	82.00
<b>Sub Metering 2</b>	1.42	6.26	0.00	78.00
<b>Sub Metering 3</b>	6.04	8.27	0.00	31.00

Table 3. Summary Statistics for Electricity Dataset

#### B.2. Intraday Volatility

**Overview** We compute 30-min realised variances (Andersen et al., 2003) for a universe of 30 different stock indices – derived using 1-min index returns subsampled from Thomson Reuters Tick History Level 1 (TRTH L1) quote data. On the whole, the entire dataset contains 1,706,709 measurements across all indices, with each trajectory spanning 17 years on average. Given the strong evidence for the intraday periodicity of returns volatility (Andersen & Bollerslev, 1997), we include the time-of-day as an additional input.

**Stock Index Identifiers (RICs):** AEX, AORD, BFX, BSESN, BVLG, BVSP, DJI, FCHI, FTMIB, FTSE, GDAXI, GSPTSE, HSI, IBEX, IXIC, KS11, KSE, MXX, N225,

NSEI, OMXC20, OMXHPI, OMXSPI, OSEAX, RUT, SMSI, SPX, SSEC, SSMI, STOXX50E

**Data Processing** From the 1-min index returns, realised variances were computed as:

$$r_k = \ln p_k - \ln p_{k-1}$$

$$y(t, 30) = \sum_{k=t-30}^t r_k^2, \quad (37)$$

where  $r_k$  is the 1-min index return at time  $k$ ,  $\ln p_k$  is the log price at  $k$ , and  $y(t, 30)$  is the 30-min realised variance at time  $t$ .

Prior to computation, the data was cleaned by only considering prices during exchange hours to avoid spurious jumps. In addition, realised variances greater than 10 times the 200-step rolling standard deviation were removed and replaced by its previous value – so as to reduce the impact of outliers.

For the experiments in Section 5, data across all stock indices were grouped together for training and testing – using data prior to 2014 for training, data between 2014-2016 for validation and data from 2016 to 4 July 2018 for independent testing. Min-max normalisation was applied to the datasets, with time normalised by the maximum trading window of each exchange and realised variances by the max and min values of the training dataset.

**Summary Statistics** A table of summary statistics can be found in Table 4 and give an indication of the general ranges of trajectories.

	Mean	S. D.	Min	Max
<b>Realised Variance*</b>	0.0007	0.0017	0.0000	0.1013
<b>Normalised Time</b>	0.43	0.27	0.00	0.97

Table 4. Summary Statistics for Volatility Dataset

### B.3. High-Frequency Stock Quotes

**Overview** This dataset consists of extracted features from TRTH L1 stock quote data for Barclays (BARC.L) – specifically forecasting microprice returns (Todd et al., 2014) using the volume imbalance as an input – comprising a total of 29,321,946 time steps between 03 January 2017 to 29 December 2017. From (Cartea et al., 2018), volume imbalance in the limit order book has been shown to be a good predictor of the direction (sign) of the next liquidity taking order, and the price changes immediately after the arrival of such an order.

**Input/Output Definitions** Microprice returns  $y_t$  are defined as:

$$p_t = \frac{V_a(t)p_b(t) + V_b(t)p_a(t)}{V_a(t) + V_b(t)}$$

$$y_t = \frac{p_t - p_{t-1}}{p_{t-1}}$$

Where  $V_b(t)$  and  $V_a(t)$  are the bid and ask volumes at time  $t$  respectively,  $p_b(t)$  and  $p_a(t)$  are the bid/ask prices, and  $p_t$  the microprice.

Volume imbalance  $I_t$  is then defined as:

$$I_t = \frac{V_b(t) - V_a(t)}{V_b(t) + V_a(t)}$$

**Data Processing** From the raw Level 1 (best bid and ask prices and volumes) data from TRTH, we isolate measurements between 08.30 to 16.00 UK time, avoiding the effects of opening and closing auctions in our forecasts. Furthermore, microprice returns were also normalised using an exponentially weighting moving standard deviation with a half life of 10,000 steps. We note that volume imbalance by definition is restricted to be  $I_t \in [-1, 1]$ , and hence does not require additional normalisation. Finally, the data was partitioned with training data from January to June, validation data from June to September, and the remainder for independent testing.

**Summary Statistics** Basic statistics can be found in Table 5, and give an indication of the range of different variables.

	Mean	S. D.	Min	Max
<b>Normalised Returns*</b>	0.00	0.80	-117.72	117.13
<b>Volume Imbalance</b>	0.02	0.48	-1.00	1.00

Table 5. Summary Statistics for Quote Dataset

## C. Hyperparameter Optimisation

**Training Details** Firstly, data trajectories were broken up into shorter segments of 50 time steps – which were randomly combined to form minibatches during training. In addition, networks were trained for up to a maximum of 100 epochs or convergence. For the electricity and volatility datasets, 50 iterations of random search were performed, using the grid found in Table 6. 20 iterations of random search were used for the quote dataset, as the significantly larger dataset led to longer training times for a given set of hyperparameters. A list of optimal hyperparameters settings are also detailed in Table 7 for reference.

**State Sizes** To ensure that consistency across all models used, we constrain both the memory state of the RNN and

	Hyperparameter Ranges
<b>Dropout Rate</b>	0.1, 0.2, 0.3, 0.4, 0.5
<b>State Size</b>	5, 10, 25, 50, 100, 150
<b>Minibatch Size</b>	256, 512, 1024
<b>Learning Rate</b>	0.0001, 0.001, 0.01, 0.1, 1.0
<b>Max Gradient Norm</b>	0.0001, 0.001, 0.01, 0.1, 1.0, 10.0

Table 6. Random Search Grid for Hyperparameter Optimisation

the latent variable modelled to have the same dimensionality – i.e.  $J = \dim(\mathbf{s}_t) = \dim(\mathbf{x}_t)$  for the RNF. The exception is the DSSM, as the full covariance matrix of the Kalman filter would result in a prohibitive  $J^2$  memory requirement if left unchecked. As such, we use the constraint where both the RNN and the Kalman filter to have the same memory capacity for the DSSM – i.e.  $J = \dim(\mathbf{s}_t) = \dim(\mathbf{x}_t) + \dim(\mathbf{x}_t)^2$ .

**Dropout Application** Across all benchmarks, dropout was applied only onto the memory state of the RNNs ( $\mathbf{h}_t$ ) in the standard fashion and not to latent states  $\mathbf{x}_t$ . For the LSTM and RNF, this corresponds to applying dropout masks to the inputs, outputs and internal states of the network. For the VRNN, DKF and DSSM, we apply dropout only to the inputs of the network – in line with (Krishnan et al., 2017).

**Sample Generation** At prediction time, latent states for the VRNN, DKF and RNF are sample as per the standard VAE case – using  $L = 1$  during training,  $L = 30$  for our validation error and  $L = 100$  for at test time. Predictions from the DSSM however were obtained directly from the mean estimates, which can be computed analytically using the Kalman filtering equations. While this differs slightly from the original paper (Rangapuram et al., 2018), it also lead to improvements in the performance DSSM by avoiding sampling errors.

	<b>LSTM</b>	<b>VRNN</b>	<b>DKF</b>	<b>DSSM</b>	<b>LG-RNF</b>	<b>NP-RNF</b>
<b>Electricity</b>						
Dropout Rate	0.1	0.1	0.1	0.3	0.4	0.3
State Size	50	50	10	25	150	25
Minibatch Size	256	256	256	512	512	256
Learning Rate	0.1	0.01	0.001	0.001	0.01	0.01
Max Norm	0.001	0.0001	0.0001	1	0.01	0.001
<b>Volatility</b>						
Dropout Rate	0.4	0.4	0.4	0.2	0.5	0.2
State Size	25	5	10	5	5	50
Minibatch Size	512	256	256	256	512	256
Learning Rate	0.01	0.001	0.001	0.01	0.001	0.001
Max Norm	1	10	10	0.001	10	1
<b>Quote</b>						
Dropout Rate	0.2	0.3	0.2	0.2	0.2	0.5
State Size	50	10	5	50	5	100
Minibatch Size	256	512	256	256	1024	1024
Learning Rate	0.01	0.01	0.001	0.01	0.1	0.01
Max Norm	1	10	1	0.0001	0.0001	1

Table 7. Optimal Hyperparameter Configuration